Bull. Mater. Sci., Vol. 39, No. 6, October 2016, pp. 1411–1418. © Indian Academy of Sciences.
DOI 10.1007/s12034-016-1298-4

Ideal shear strength and deformation behaviours of $L1_0$ TiAl from first-principles calculations

PING-YING TANG*, GUO-HUA HUANG, QING-LIAN XIE and JIAN-YING LI
Key Laboratory of New Electric Functional Materials of Guangxi Colleges and Universities,
Guangxi Teachers Education University, Nanning 530023, China

MS received 18 October 2014; accepted 11 April 2016

Abstract. **The stress–strain relationships for four different shear processes of $L1_0$ TiAl have been investigated from first-principles calculations, and the peak shear stresses in these slip systems were obtained. By analysing the structural unit cell, bond length and charge density, the deformation modes under shear were elaborately discussed. Both of the peak shear stresses and the charge density indicate that the ideal shear strength of $L1_0$ TiAl occurs in the $\langle 11\bar{2}]\{111\}$ direction. It is shown that some bonds are enormously stretched accompanying with depletion of charge density as the strain increase. The density of states was studied in detail. It is indicated that strong hybridization exists between Ti 3*d* and Al 2*p*, and the structural stability would be lowered with increase of the strain.**

Keywords. **First-principles calculations; ideal shear strength; deformation mode; charge density; density of states.**

1. Introduction

TiAl intermetallic compound with an ordered $L1_0$ (space group *P4/mmm*, prototype CuAu) crystal structure is a potential high temperature structural material for aerospace and automotive applications, due to its high melting points, low density, high strength, and good oxidation and creep resistance [1–3]. However, practical application of TiAl is still hindered by its poor ductility at room temperature [4–6], which is often associated with an insufficient number of slip systems to satisfy the von Mises criterion for slip deformation of polycrystalline materials [7,8]. In order to utilize it fully, a basic understanding of the micro-mechanisms of plasticity and fracture behaviours under deformation is required.

Based on a detailed analysis of the topography of the single crystal yield surface, a deformation mode map for slip and twinning of $L1_0$ TiAl was derived by Mecking *et al* [9]. Various deformation modes, occurring during the plastic deformation processes of $L1_0$ TiAl, have been extensively characterized by transmission electron microscopy [10–20]. Recently, the compressive deformation behaviour of porous $L1_0$ TiAl with directional pores was investigated by Ide *et al* [21]. Zhang *et al* [22] studied the dependence of heating rate in PCAS (pulse current auxiliary sintering apparatus) on microstructures and high temperature deformation properties of $L1_0$ TiAl. Zambaldi and Raabe [23] presented a nanoindentation analysis combining experimental and computational method, and developed a method to assess the activation of competing deformation mechanisms.

Several theoretical calculations have been performed to study the mechanical properties of $L1_0$ TiAl, involving the deformation, fracture behaviour and dislocations etc. Atomistic simulations of dislocation configurations of $L1_0$ TiAl were investigated using embedded-atom method potentials [24,25]. The deformation and fracture behaviour were studied by Yoo *et al* [26] using the linear elastic theory. They claimed that the coupling effect due to elastic incompatibility reduces the misfit strain at the interface when a tensile stress is applied normal to it. Recently, the dynamic shear deformation process was investigated by Liu *et al* [27] using the theory of dislocation nucleation and mobility. It is found that among the shear directions in $L1_0$ TiAl, $1/6\langle 11\bar{2}\rangle$ slip possesses lower peak shear strength than $1/2\langle 1\bar{1}0\rangle$ slip, and the $1/2\langle 1\bar{1}0]$ dislocation can decompose into two $1/6\langle 11\bar{2}\rangle$ partial dislocations. However, the deformation mechanisms at the electronic and atomic levels are still not clear. Particularly, combined with an analysis of the underlying electronic and atomic processes, studies of the ideal shear strength are valuable and allow deep insights into fundamental aspects of deformation modes.

A full understanding of the ideal shear strength would require an examination of the shear stress–strain relation of the material under large deformation loading conditions. Whereas, the stress response may become nonlinear at large strains, which could lead to strength anisotropy that cannot be predicted by elastic constants determined at equilibrium structure. So a more stringent test is provided by the lowest peak stress (ideal shear strength) in shear stress–strain relation. A perfect crystal would become mechanically unstable at the lowest peak stress, which sets an upper bound for material strength. As the non-unity of c/a in $L1_0$ TiAl, the shear stress–strain relations in $\langle 1\bar{1}0]\{111\}$, $\langle 0\bar{1}1]\{111\}$,

*Author for correspondence (tangpy801@163.com)

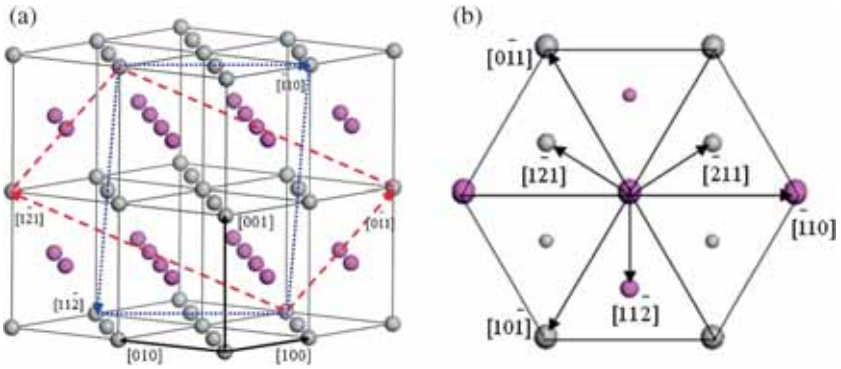

Figure 1. (**a**) Geometries of shear for $L1_0$ TiAl in $\langle 1\bar{1}0\rangle\{111\}$, $\langle 11\bar{2}\rangle\{111\}$, $\langle 0\bar{1}1\rangle\{111\}$ and $\langle 1\bar{2}1\rangle\{111\}$ slip systems. (**b**) The {111} plane configuration. Grey atoms are Ti and pink atoms are Al, and the atoms with different sizes represent the arrangements on different planes.

$\langle 11\bar{2}\rangle\{111\}$ and $\langle 1\bar{2}1\rangle\{111\}$ slip systems were investigated by first-principles calculations in this article. The ideal shear strength and deformation mode under shear for $L1_0$ TiAl were studied and discussed in detail, together with elaborate density of states (DOS) analysis.

2. Structural model and computational method

The common slip systems for $L1_0$ TiAl are plotted in figure 1a. The {111} plane configuration of $L1_0$ TiAl is also schematically shown in figure 1b, in which the shear directions considered in this article are also marked. The shear strength calculations were carried out using the Vienna ab initio simulation package [28] code based on density functional theory. The electron–ion interactions were treated by the projector augment wave method [29] and the exchange–correlation term was described by the generalized gradient approximation [30]. The total energy of the structures was minimized by relaxing the structural parameters using a quasi-Newton method [31]. The total energy and stress calculations used a 320 eV energy cutoff and a $10 \times 6 \times 8$, $10 \times 6 \times 8$, $6 \times 10 \times 8$ and $6 \times 10 \times 8$ Monkhorst-Pack [32] k-point grid for $\langle 1\bar{1}0\rangle\{111\}$, $\langle 0\bar{1}1\rangle\{111\}$, $\langle 11\bar{2}\rangle\{111\}$ and $\langle 1\bar{2}1\rangle\{111\}$ slip systems, respectively. The convergence test showed that the error for the total energy is less than 1 meV per atom and the residual stresses in the fully relaxed structures is less than 0.1 GPa. The electronic total energy calculations were performed by means of tetrahedron method with Blöchl corrections [33].

As described in detail elsewhere [34,35], the shear stress–strain relations were calculated by incrementally deforming the modelled cell in the direction of the applied strain. At each step, the atomic basis vectors perpendicular to the applied strain are simultaneously relaxed until the other stress components vanish. Meanwhile, all the internal freedoms of the atom are relaxed until the forces on each atom becomes negligible. To ensure that the strain path is continuous, the starting position at each strain step has been taken from the relaxed coordinates of the previous strain step. The obtained total energies are fitted by smooth energy–strain curves. From these energy–strain fit curves, the shear stress can be calculated by $\tau = [1/V(\gamma)]\partial E/\partial\gamma$, where γ is the true strain. The ideal shear strength is the lowest peak shear stress, which is the first maximum in the shear stress–strain curve.

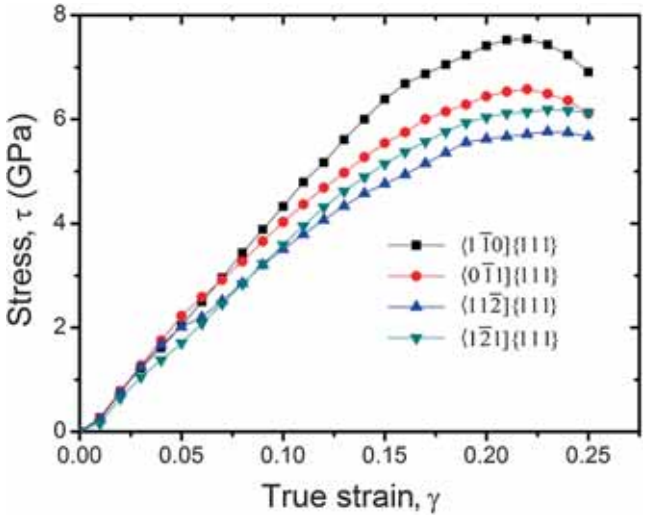

Figure 2. Calculated shear stress–strain relations for $L1_0$ TiAl in different slip systems.

3. Results and discussion

3.1 *Ideal shear strength*

The stress–strain relations for $\langle 1\bar{1}0\rangle\{111\}$, $\langle 0\bar{1}1\rangle\{111\}$, $\langle 11\bar{2}\rangle\{111\}$ and $\langle 1\bar{2}1\rangle\{111\}$ shear processes of $L1_0$ TiAl are shown in figure 2. At small strains (≤ 0.02), the stresses of these slip systems are almost the same. As the strain increases, the stresses of $\langle 1\bar{1}0\rangle\{111\}$ and $\langle 0\bar{1}1\rangle\{111\}$ slip systems are

Table 1. Peak shear stresses for $L1_0$ TiAl in different slip systems, together with other theoretical data.

Slip system	$\langle 1\bar{1}0\rangle\{111\}$	$\langle 0\bar{1}1\rangle\{111\}$	$\langle 11\bar{2}\rangle\{111\}$	$\langle 1\bar{2}1\rangle\{111\}$
Peak shear stress (GPa)	7.54	6.57	5.76	6.19[a]
	10.21	7.79	4.30	5.61[b]
Critical shear strain	0.22	0.22	0.23	0.23[a]

[a]This work; [b]Ref. [27].

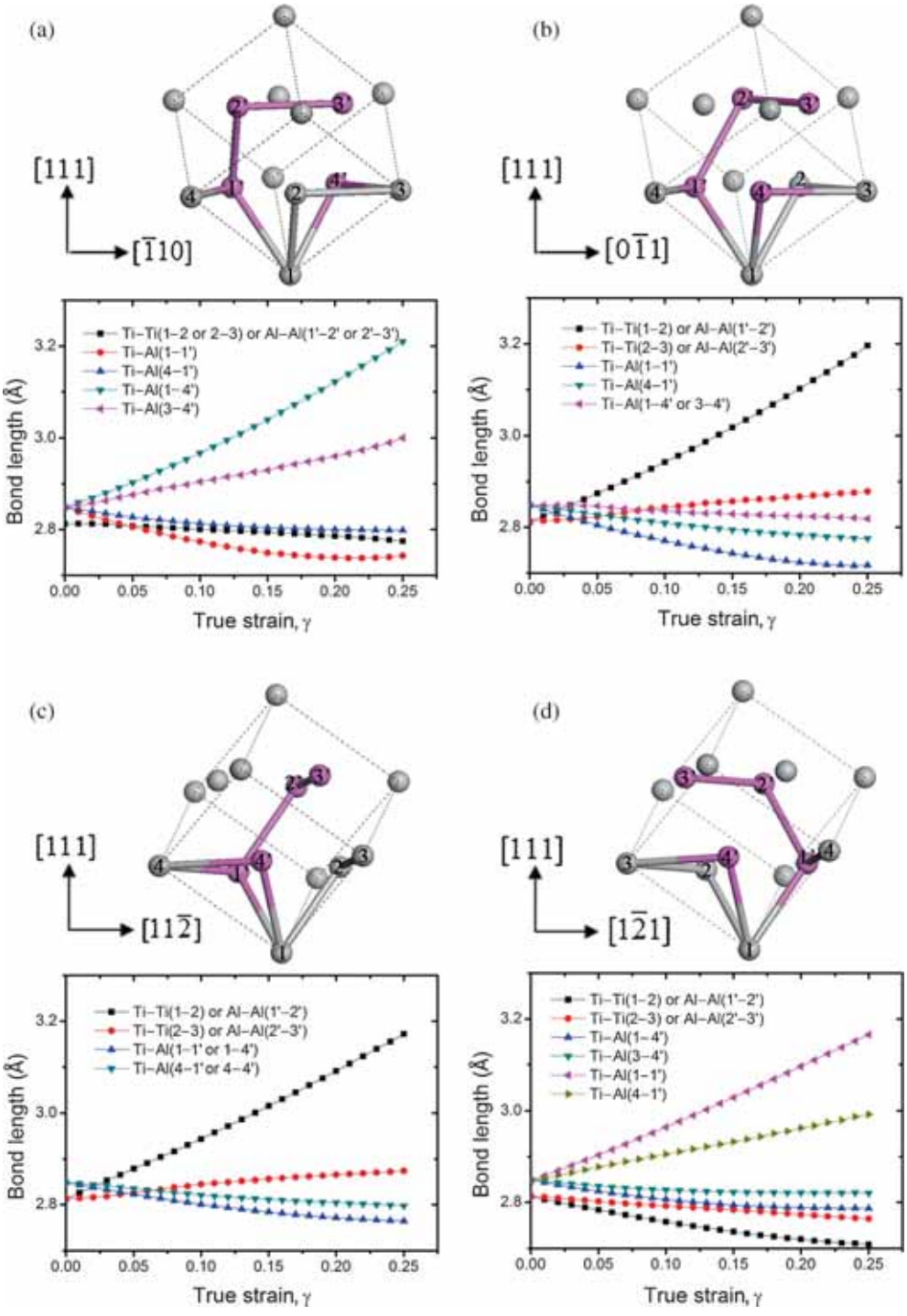

Figure 3. The structural unit cell and the bond length *vs*. true strain for (**a**) $\langle 1\bar{1}0\rangle\{111\}$, (**b**) $\langle 0\bar{1}1\rangle\{111\}$), (**c**) $\langle 11\bar{2}\rangle\{111\}$ and (**d**) $\langle 1\bar{2}1\rangle\{111\}$ slip systems.

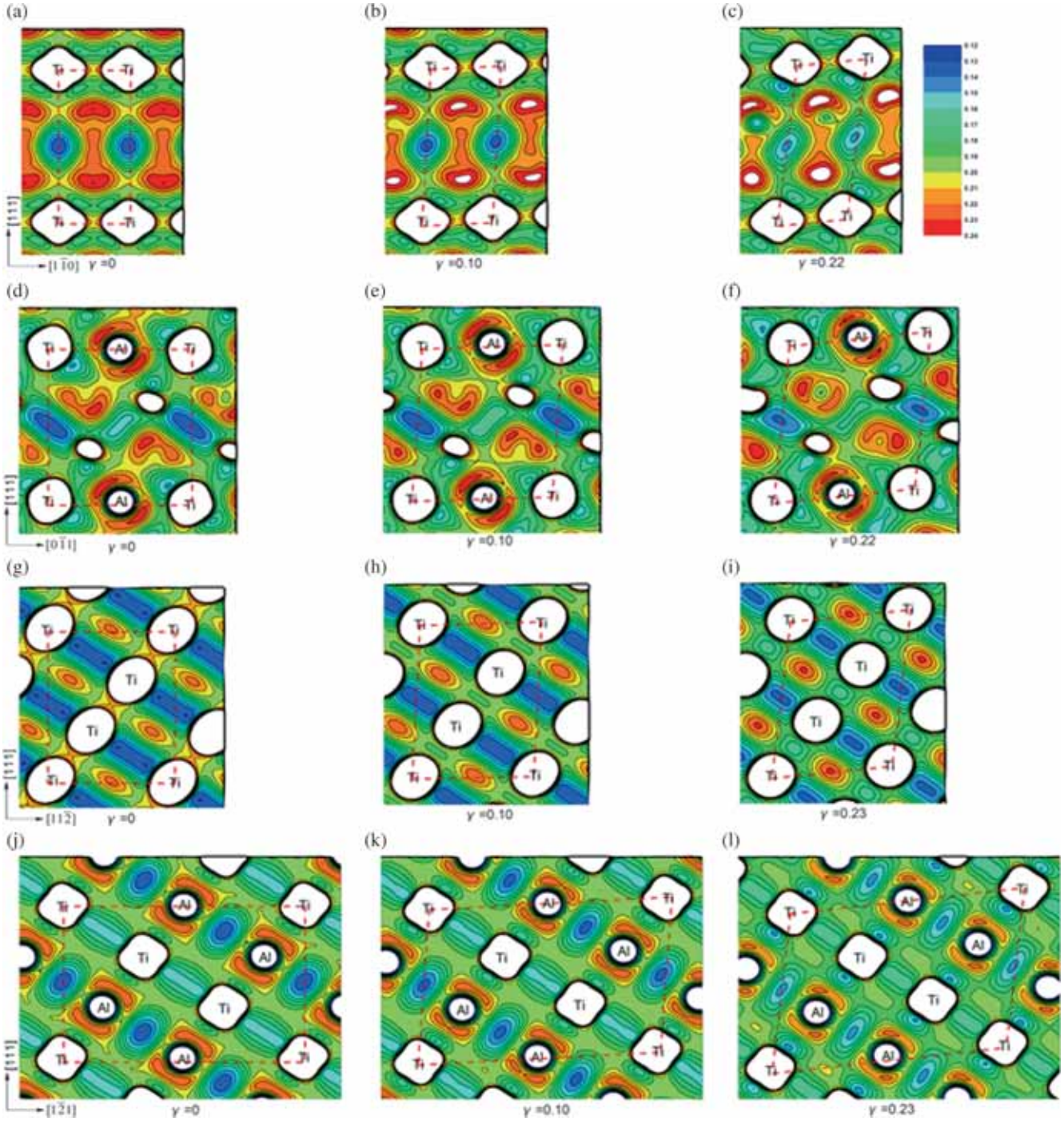

Figure 4. The development of the contour plots charge density of $L1_0$ TiAl for (**a–c**) $\langle 1\bar{1}0]\{111\}$, (**d–f**) $\langle 0\bar{1}1]\{111\}$, (**g–i**) $\langle 11\bar{2}]\{111\}$ and (**j–l**) $\langle 1\bar{2}1]\{111\}$ slip systems at various strains.

larger than those of $\langle 1\bar{2}1]\{111\}$ and $\langle 11\bar{2}]\{111\}$ slip systems. At strain range 0.02–0.06, the stresses of $\langle 1\bar{1}0]\{111\}$ are slightly smaller than that of $\langle 0\bar{1}1]\{111\}$. Whereas at strains greater than 0.06, the stresses of $\langle 1\bar{1}0]\{111\}$ are much larger than that of $\langle 0\bar{1}1]\{111\}$. Interestingly, similar tendency can be found between $\langle 1\bar{2}1]\{111\}$ and $\langle 11\bar{2}]\{111\}$ slip systems. The stresses of $\langle 1\bar{2}1]\{111\}$ are smaller than that of $\langle 11\bar{2}]\{111\}$ at strains between 0.02 and 0.08, and at strains greater than 0.08 the stresses of $\langle 1\bar{2}1]\{111\}$ are larger than that of $\langle 11\bar{2}]\{111\}$.

The peak shear stresses of $L1_0$ TiAl are listed in table 1, together with available theoretical data. The calculated peak shear stresses decrease in the sequence of $\langle 1\bar{1}0]\{111\}$, $\langle 0\bar{1}1]\{111\}$, $\langle 1\bar{2}1]\{111\}$ and $\langle 11\bar{2}]\{111\}$ with corresponding strengths of 7.54, 6.57, 6.19 and 5.76 GPa, respectively. Obviously, this sequence is in good accordance with that

calculated by Liu *et al* [27]. The calculated results indicate that the ideal shear strength of $L1_0$ TiAl appears in the $\langle 11\bar{2}\rangle\{111\}$ shear direction by virtue of the lowest peak shear stress. For $\langle 1\bar{1}0\rangle\{111\}$ and $\langle 0\bar{1}1\rangle\{111\}$ slip systems, the critical shear strain corresponding to the peak shear stress is 0.22, and $\langle 11\bar{2}\rangle\{111\}$ and $\langle 1\bar{2}1\rangle\{111\}$ slip systems would get their stress maxima at 0.23 critical shear strain.

3.2 *Deformation mode under shear*

To reveal the mechanisms and trends for structural deformation in $L1_0$ TiAl, the local bonding arrangements and atomistic deformation modes under shear loading were investigated in detail. Figure 3 presents the structural unit cell and the bond length verse true strain for $\langle 1\bar{1}0\rangle\{111\}$, $\langle 0\bar{1}1\rangle\{111\}$, $\langle 11\bar{2}\rangle\{111\}$ and $\langle 1\bar{2}1\rangle\{111\}$ slip systems. There are two types of Ti–Ti (or Al–Al) bonds and four types of Ti–Al bonds in $L1_0$ TiAl. As shown in figure 3, the Ti–Ti (or Al–Al) bonds are marked as 1–2 (or 1′–2′) and 2–3 (or 2′–3′), and the Ti–Al bonds are marked as 1–1′, 4–1′, 1–4′ and 3–4′. The orientation of the bond and the bond length variation in different slip system are different.

The calculated bond length *vs*. true strain indicates that with the increase in strain the most significantly stretched bond is 1–4′ Ti–Al bond for $\langle 1\bar{1}0\rangle\{111\}$ slip system, 1–2 Ti–Ti (or 1′–2′ Al–Al) bond for $\langle 0\bar{1}1\rangle\{111\}$ slip system, 1–2 Ti–Ti (or 1′–2′ Al–Al) bond for $\langle 11\bar{2}\rangle\{111\}$ slip system and 1–1′ Ti–Al bond for $\langle 1\bar{2}1\rangle\{111\}$ slip system, respectively. As can be seen from figure 3, the orientations of these most significantly stretched bonds for different slip system in mapping plane are similar to each other. Moreover, the 3–4′ Ti–Al bond, 2–3 Ti–Ti (or 2′–3′Al–Al) bond, 2–3 Ti–Ti (or 2′–3′Al–Al) bond and 4–1′ Ti–Al bond for $\langle 1\bar{1}0\rangle\{111\}$, $\langle 0\bar{1}1\rangle\{111\}$, $\langle 11\bar{2}\rangle\{111\}$ and $\langle 1\bar{2}1\rangle\{111\}$ slip systems, respectively, are also stretched as the strain increases. Obviously, these bonds in mapping plane also have a similar direction, while all the other bonds in slip system are shrunk with increase of the strain. It is indicated that 1–4′ Ti–Al bond for $\langle 1\bar{1}0\rangle\{111\}$ slip system, 1–2 Ti–Ti (or 1′–2′ Al–Al) bond for $\langle 0\bar{1}1\rangle\{111\}$ slip system, 1–2 Ti–Ti (or 1′–2′ Al–Al) bond for $\langle 11\bar{2}\rangle\{111\}$ slip system and 1–1′ Ti–Al bond for $\langle 1\bar{2}1\rangle\{111\}$ slip system are enormously stretched up to the critical shear strain where the stress reaches a maximum, and then these bonds break and the stress starts to decrease at larger strain.

Figure 4 plots the contour plots of charge density distribution of $L1_0$ TiAl for $\langle 1\bar{1}0\rangle\{111\}$, $\langle 0\bar{1}1\rangle\{111\}$, $\langle 11\bar{2}\rangle\{111\}$ and $\langle 1\bar{2}1\rangle\{111\}$ slip systems at various strains. The charge accumulation between atoms for $(11\bar{2})$ plane under $\langle 1\bar{1}0\rangle\{111\}$ shear strain is most remarkable, and then followed by $(\bar{2}11)$ plane under $\langle 0\bar{1}1\rangle\{111\}$ shear strain, $(\bar{1}01)$ plane under $\langle 1\bar{2}1\rangle\{111\}$ shear strain and $(1\bar{1}0)$ plane under

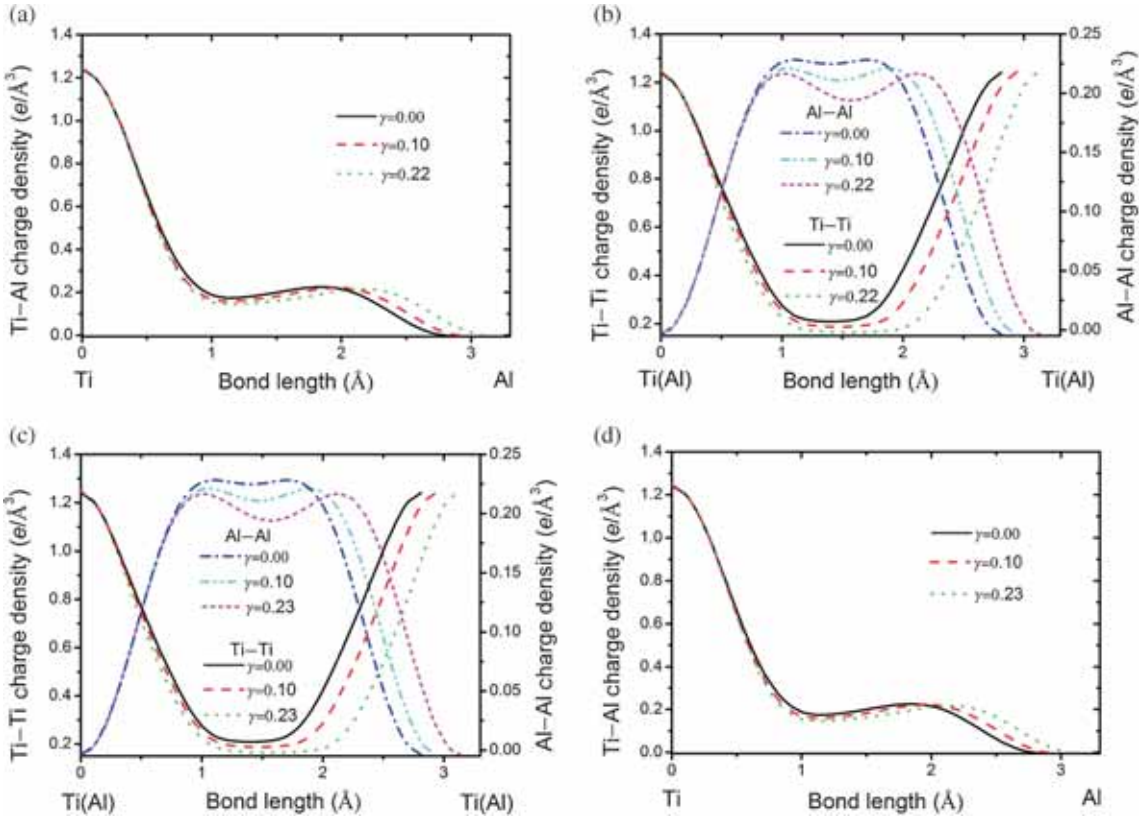

Figure 5. Charge density along the bonds of 1–4′ Ti–Al for (**a**) $\langle 1\bar{1}0\rangle\{111\}$, (b) 1–2 Ti–Ti (or 1′–2′ Al–Al) for $\langle 0\bar{1}1\rangle\{111\}$, (**c**) 1–2 Ti–Ti (or 1′–2′ Al–Al) for $\langle 11\bar{2}\rangle\{111\}$ and (**d**) 1–1′ Ti–Al for $\langle 1\bar{2}1\rangle\{111\}$ slip systems at various strains.

$\langle 11\bar{2}]\{111\}$ shear strain. In general, the more interatomic charge the more interaction between atoms and the higher strength of the material. Therefore, the peak shear stress of $L1_0$ TiAl for $\langle 1\bar{1}0]\{111\}$ slip system is the highest, and then followed by $\langle 0\bar{1}1]\{111\}$ slip system, $\langle 1\bar{2}1]\{111\}$ slip system and $\langle 11\bar{2}]\{111\}$ slip system, which is consistent with the results obtained from peak shear stresses. For all of these four slip systems, with increase in the shear strain, the charge density along shear direction gradually decreases, which means the interaction between atoms along shear

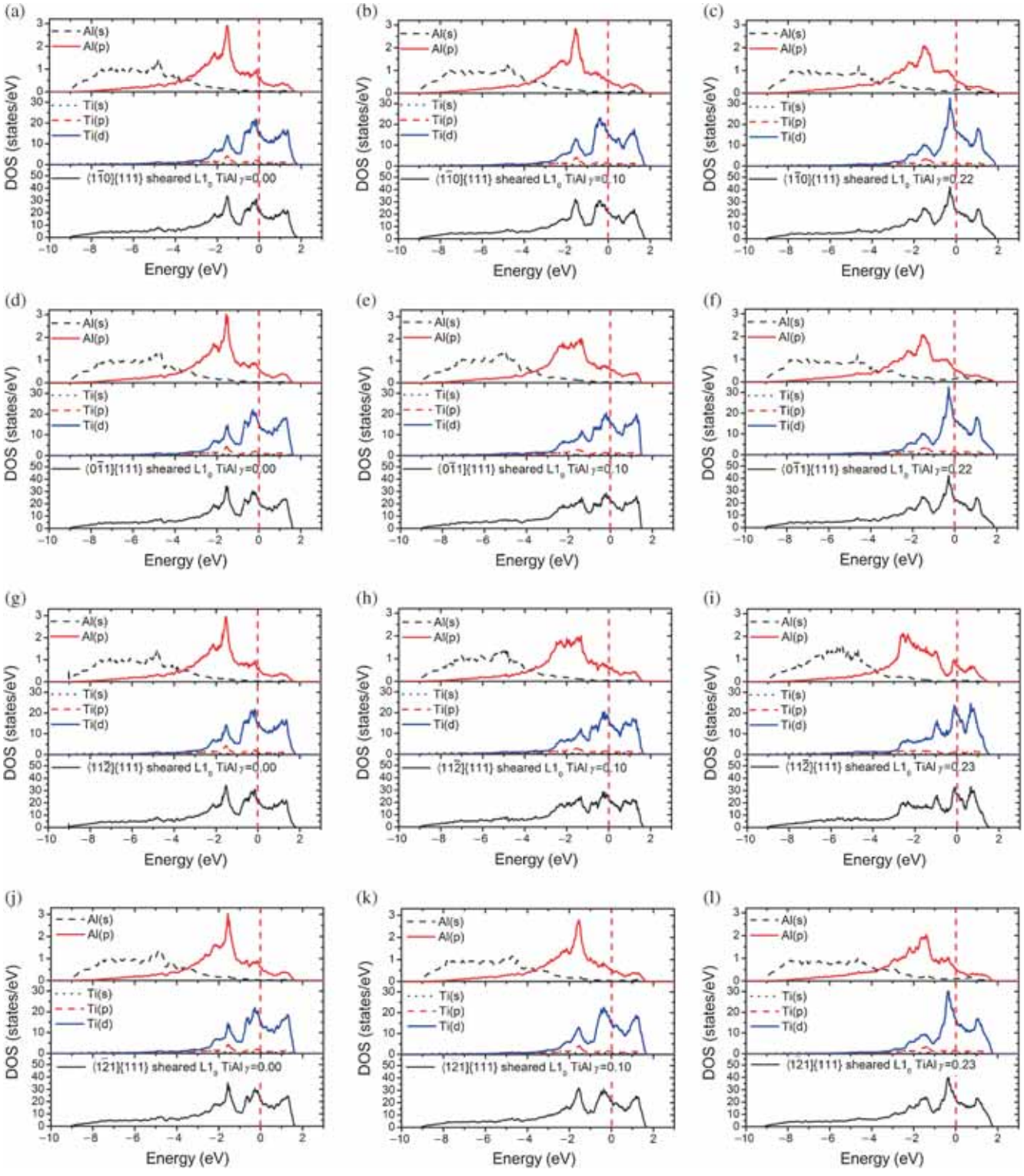

Figure 6. The total and partial density of states (DOS) of $L1_0$ TiAl for (**a–c**) $\langle 1\bar{1}0]\{111\}$, (**d–f**) $\langle 0\bar{1}1]\{111\}$, (**g–i**) $\langle 11\bar{2}]\{111\}$ and (**j–l**) $\langle 1\bar{2}1]\{111\}$ slip systems at various strains.

direction is weakened. The charge density perpendicular to the shear direction gradually increases, which shows that the interaction between atoms perpendicular to shear direction is strengthened.

In order to gain more insight into the bonding behaviour and the shear deformation process, the charge density along the greatest stretched bond for $\langle 1\bar{1}0]\{111\}$, $\langle 0\bar{1}1]\{111\}$, $\langle 11\bar{2}]\{111\}$ and $\langle 1\bar{2}1]\{111\}$ slip systems at various strains are plotted in figure 5. Figure 5a illustrates the 1–4′ Ti–Al charge density for $\langle 1\bar{1}0]\{111\}$ slip system at $\gamma = 0.00$, 0.10 and 0.22 strains. It is clearly seen that charge highly accumulates around Ti atom and Ti–Al bond exhibits covalent characters. With increase in the strain, the charge density along 1–4′ Ti–Al bond gradually decreases. It is indicated that the interaction between 1 Ti and 4′ Al is weakened with strain increase. 1–2 Ti–Ti (or 1′–2′ Al–Al) charge density for $\langle 0\bar{1}1]\{111\}$ slip system at $\gamma = 0.00$, 0.10 and 0.22 strains are shown in figure 5b. As can bee seen that Ti–Ti belongs to metallic bond and Al–Al is covalent bond. It is demonstrated that the interaction between 1 Ti and 2 Ti (or 1′ Al and 2′ Al) is weakened with strain increase as the charge density along 1–2 Ti–Ti (or 1′–2′ Al–Al) bond gradually depletes. Figure 5c presents the 1–2 Ti–Ti (or 1′–2′ Al–Al) charge density for $\langle 11\bar{2}]\{111\}$ slip system at $\gamma = 0.00$, 0.10 and 0.23 strains. It is also shown that the interaction of the metallic 1–2 Ti–Ti (or covalent 1′–2′ Al–Al) bond is weakened with increase in the strain as the charge density along 1–2 Ti–Ti (or 1′–2′ Al–Al) bond gradually reduces. 1–1′ charge density for $\langle 1\bar{2}1]\{111\}$ slip system at $\gamma = 0.00$, 0.10 and 0.23 strains are displayed in figure 5d. With the depletion of charge density along covalent 1–1′ Ti–Al bond, the interaction between 1 Ti and 1′ Al is weakened too as the strain increase.

3.3 *Density of states*

To better analyse the nature of bonding, and especially to look into the close relationship between electronic structure and mechanical properties, the total and partial DOS of $L1_0$ TiAl in $\langle 1\bar{1}0]\{111\}$, $\langle 0\bar{1}1]\{111\}$, $\langle 11\bar{2}]\{111\}$ and $\langle 1\bar{2}1]\{111\}$ slip systems at various strains were investigated. As shown in figure 6, the total and partial DOS of these four slip systems exhibit very similar characteristics as a whole. A general feature of these figures is that the Fermi energy (E_F), which is set at energy zero and marked by the vertical lines, lies directly in the pseudo-gap of the DOS, indicating that there is a noticeable covalent contribution to the bonding. For the DOS of unstrained $L1_0$ TiAl, the states, located between -9.0 and -4.0 eV, dominantly consist of Al 2*s* orbitals. The states, ranged from -4.0 to -0.8 eV below the Fermi level, are composed of Ti 3*d*–Al 2*p* bonding orbitals, showing strong hybridization between Ti 3*d* and Al 2*p*. The states above -0.8 eV mainly originate from Ti 3*d* orbitals. For all of these four slip systems, with increase in the strain the total DOS at the Fermi level gradually increase, indicating that the shear deformed structures would lower the stability. When examining the fine structures of DOS of strained $L1_0$ TiAl, a common feature would be found for all of these four slip systems; that is, the DOS move towards the higher energy region as the strain increase, meaning more unstable than ever.

4. Conclusion

First-principles calculations were implemented to investigate the stress–strain relationships for $\langle 1\bar{1}0]\{111\}$, $\langle 0\bar{1}1]\{111\}$, $\langle 11\bar{2}]\{111\}$ and $\langle 1\bar{2}1]\{111\}$ shear processes of $L1_0$ TiAl. The peak shear stresses in four slip systems were obtained and in good accordance with other theoretical work. The deformation behaviours under shear were extensively discussed by means of structural unit cell, bond length and charge density. Both of the peak shear stresses and charge density indicate that the ideal shear strength of $L1_0$ TiAl occurs in the $\langle 11\bar{2}]\{111\}$ direction. It is shown that, with increase in the strain, some bonds are significantly stretched accompanying with depletion of charge density. Furthermore, the charge density demonstrates the covalent feature of Ti–Al and Al–Al bonds, and the Ti–Ti bond is metallic. The detailed study of DOS reveals that a strong hybridization exists between Ti 3*d* and Al 2*p*. In addition, the stability of the structure lowers with increase in the strain.

Acknowledgements

This study was supported by the National Natural Science Foundation of China (No. 51561005), Natural Science Foundation of Guangxi Province (2013GXNSFBA19007), Key Project of Guangxi Universities Scientific Research (2013ZD039) and Key Laboratory of New Electric Functional Materials of Guangxi Colleges and Universities.

References

[1] Kim Y W 1989 *J. Met.* **41** 24
[2] Morris M A and Leboeuf M 1997 *Mater. Sci. Eng. A* **239–240** 429
[3] Zhang W J, Reddy B V and Deevi S C 2001 *Scripta Mater.* **45** 645
[4] Huang S C and Hall E L 1991 *Acta Metall.* **39** 1053
[5] Song Y, Xu D S, Yang R, Li D and Hu Z Q 1998 *Intermetallics* **6** 157
[6] Kawabata T, Fukai H and Izumi O 1998 *Acta Mater.* **46** 2185
[7] von Mises R 1928 *Z. Angew. Math. Mech.* **8** 161
[8] Schwarz R B, Desch P B, Srinivasan S and Nash P 1992 *Nanostruct. Mater.* **1** 37
[9] Mecking H, Hartig C and Kocks U F 1996 *Acta Mater.* **44** 1309
[10] Vasudevan V K, Stucke M A, Court S A and Fraser H L 1989 *Philos. Mag. Lett.* **59** 299
[11] Inui H, Oh M H and Nakamura A 1992 *Acta Metall.* **40** 3095
[12] Morris M A 1993 *Philos. Mag. A* **68** 237
[13] Kishida K, Inui H and Yamaguchi M 1998 *Philos. Mag. A* **78** 1

[14] Appel F and Christoph U 1999 *Intermetallics* **7** 1173
[15] Gibson M A and Forwood C T 2000 *Philos. Mag. A* **80** 2747
[16] Forwood C T and Gibson M A 2000 *Philos. Mag. A* **80** 2785
[17] Gibson M A and Forwood C T 2002 *Philos. Mag. A* **82** 1381
[18] Couret A, Calderon H A and Veyssière P 2003 *Philos. Mag.* **83** 1699
[19] Liu Y, Lin D L, Liu Z G and Wang Z G 1999 *Philos. Mag. A* **79** 2965
[20] Appel F 2005 *Philos. Mag.* **85** 205
[21] Ide T, Tane M and Nakajima H 2009 *Mater. Sci. Eng. A* **508** 220
[22] Zhang C P, Zhang K F and Wang G F 2010 *Intermetallics* **18** 834
[23] Zambaldi C and Raabe D 2010 *Acta Mater.* **58** 3516
[24] Simmons J P, Rao S I and Dimiduk D M 1997 *Philos. Mag. A* **75** 1299
[25] Panova J and Farkas D 1998 *Philos. Mag. A* **78** 389
[26] Yoo M H, Zou J and Fu C L 1995 *Mater. Sci. Eng. A* **192** 14
[27] Liu Y L, Liu L M, Wang S Q and Ye H Q 2007 *Intermetallics* **15** 428
[28] Kresse G and Furthmüller J 1996 *Phys. Rev. B* **54** 11169
[29] Blöchl P E 1994 *Phys. Rev. B* **50** 17953
[30] Perdew J P, Burke K and Ernzerhof M 1996 *Phys. Rev. Lett.* **77** 3865
[31] Pfrommer B G, Côté M, Louie S G and Cohen M L 1997 *J. Comput. Phys.* **131** 233
[32] Monkhorst H J and Pack J D 1976 *Phys. Rev. B* **13** 5188
[33] Blöchl P E, Jepsen O and Andersen O K 1994 *Phys. Rev. B* **49** 16223
[34] Roundy D, Krenn C R, Cohen M L and Morris J W 1999 *Phys. Rev. Lett.* **82** 2713
[35] Roundy D, Krenn C R, Cohen M L and Morris J W 2001 *Philos. Mag. A* **81** 1725